UCSF

Title

[11C]Para-Aminobenzoic Acid: A Positron Emission Tomography Tracer Targeting Bacteria-Specific Metabolism

Permalink

https://escholarship.org/uc/item/9xt730sz

Journal

ACS Infectious Diseases, 4(7)

ISSN

2373-8227

Authors

Mutch, Christopher A
Ordonez, Alvaro A
Qin, Hecong
et al.

Publication Date

2018-07-13

DOI

10.1021/acsinfecdis.8b00061

Peer reviewed

[11C]PABA: A PET tracer targeting bacteria-specific metabolism

Christopher A. Mutch[1], **Alvaro A. Ordonez**[2], **Hecong Qin**[1], **Matthew Parker**[1], **Lauren E. Bambarger**[2], **Javier E. Villanueva-Meyer**[1], **Joseph Blecha**[1], **Valerie Carroll**[1], **Celine Taglang**[1], **Robert Flavell**[1], **Renuka Sriram**[1], **Henry VanBrocklin**[1], **Oren Rosenberg**[3], **Michael A. Ohliger**[1,4], **Sanjay K. Jain**[2,*], **Kiel D. Neumann**[5,*], and **David M. Wilson**[1,*]

[1]Department of Radiology and Biomedical Imaging, University of California, San Francisco, San Francisco, CA 94158, USA

[2]Center for Infection and Inflammation Imaging Research, Department of Pediatrics, Johns Hopkins University School of Medicine, Baltimore, MD 21287, USA

[3]Department of Medicine, University of California, San Francisco, San Francisco, CA 94158, USA

[4]Department of Radiology, Zuckerberg San Francisco General Hospital, San Francisco CA 94110, USA

[5]Department of Radiology and Medical Imaging, University of Virginia, Charlottesville, VA 22903, USA

Abstract

Imaging studies are frequently used to support the clinical diagnosis of infection. These techniques include computed tomography (CT) and magnetic resonance imaging (MRI) for structural information, and single photon emission computed tomography (SPECT) or positron emission tomography (PET) for metabolic data. However, frequently there is significant overlap in the imaging appearance of infectious and non-infectious entities using these tools. To address this concern, recent approaches have targeted bacteria-specific metabolic pathways. For example, radiolabelled sugars derived from sorbitol and maltose have been investigated as PET radiotracers, since these are efficiently incorporated into bacteria but are poor substrates for mammalian cells. We have previously shown that para-aminobenzoic acid (PABA) is an excellent candidate for development as a bacteria-specific imaging tracer as it is rapidly accumulated by a wide range of pathogenic bacteria, including metabolically quiescent bacteria and clinical strains, but not by

mammalian cells. Therefore, in this study we developed an efficient radiosynthesis for [^{11}C]PABA, investigated its accumulation into *Escherichia coli* and *Staphylococcus aureus* laboratory strains *in vitro*, and shown that it can distinguish between infection and sterile inflammation in a murine model of acute bacterial infection.

Graphical Abstract
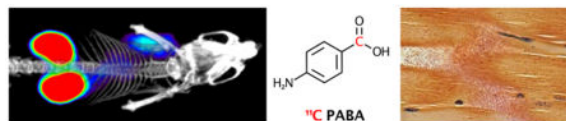
Keywords

infection; positron emission tomography; metabolism; folate; bacteria

Suspected bacterial infection is a frequent indication for imaging studies in clinical practice. Current techniques rely heavily on secondary inflammatory changes to localize disease. These changes include increased blood flow and vascular permeability in contrast-enhanced computed tomography (CT) and magnetic resonance imaging (MRI), increased glucose utilization in positron emission tomography using [^{18}F]fluorodeoxyglucose (FDG-PET) and recruitment of leukocytes in tagged white blood cell (WBC) nuclear medicine studies[1,2]. While these studies are generally sensitive for infection in immunocompetent patients, they rely on indirect methods for detection of infection, limiting specificity. These exams are also difficult to interpret when infection is suspected in the setting of recent surgery, trauma or malignancy[3]. Additionally, they can be falsely negative when patients are unable to mount a sufficient response to infection as is often the case in immunosuppressed or immunodeficient patients[4,5]. While antibiotics are critical in the case of a true infection, they are not useful for the management of sterile inflammation or other infection mimics and may in fact be harmful leading to side effects, risk of generating antibiotic-resistant strains, and disruption of the normal microbiome[6]. In this era of increasing antibiotic resistance, especially with health care-associated infections, treatment with broad spectrum antibiotics contributes to the public health emergency of antibiotic resistance[7].

These concerns have motivated the investigation of imaging methods targeting bacteria-specific metabolic pathways, especially using clinically translatable technologies such as PET or MRI[8,9]. Recent studies have shown bacterial uptake of radiolabelled sugars and sugar alcohols that are not efficiently metabolized by humans, such as 2-deoxy-2-[^{18}F]fluorosorbitol (^{18}F-FDS), 6-[^{18}F]fluoromaltose, and 6″-[^{18}F]fluoromaltotriose[10–12]. Other innovative approaches target bacterial iron metabolism via ^{67}Ga or ^{68}Ga-siderophore complexes[13–15]. Recently we also showed that a D-amino acid derived tracer D-[methyl-^{11}C]methionine ([^{11}C]D-Met) could distinguish active infection from sterile inflammation in a murine myositis model, presumably via incorporation into bacterial peptidoglycan[16]. These tracers show strong clinical potential, but may be limited by differing ability of particular bacterial strains to utilize these substrates. For example, ^{18}F-FDS is accumulated by gram-negative, Enterobacteriaceae only. This may represent a major

advantage for determining organism type (and tailoring appropriate antimicrobial therapy), but would be potentially limiting in infections due to other bacteria. Thus, it is important to identify additional potential targets for imaging of infection.

One compelling target is bacterial folate biosynthesis. Folate is a key component of many metabolic pathways in both prokaryotes and eukaryotes including DNA and amino acid synthesis. Bacteria and mammals incorporate folate via divergent mechanisms. While bacteria are able to produce their own folate, humans must obtain it through their diets. Because of its crucial role in bacteria, folate biosynthesis has long been an important target for antibiotics, such as sulfonamides, which act as competitive inhibitors of bacterial dihydropteroate synthase through their structural similarity to PABA, the key precursor to dihydrofolate[17]. Inhibitors of bacterial dihydrofolate reductase have also been developed, including trimethoprim which was recently radiolabeled for imaging infection in preclinical models[18]. The uptake and incorporation pathway of PABA in bacteria is shown in Figure 1. Meanwhile, mammals lack the enzymatic machinery to utilize PABA and rapidly eliminate it through primarily urinary excretion. PABA is U.S. Food and Drug Administration (FDA) approved as a sunscreen and an oral medication, and thus its safety in humans is well-established[19]. These qualities and results from our prior studies led us to hypothesize that radio-labelled PABA would be an excellent candidate for imaging bacterial infections[20]. Moreover, we have also demonstrated, via commercially available [^{3}H]PABA, rapid incorporation (minutes) into an extended bacterial panel of laboratory strains, and clinical isolates including multidrug resistant organisms (MDROs) such as methicillin-resistant *Staphylococcus aureus* (MRSA), extended-spectrum beta-lactamase (ESBL)-producing *Escherichia coli* and carbapenem-resistant Enterobacteriaceae (CRE) strains[20]. Finally, PABA uptake in bacteria is high regardless of growth phase, accumulated by stationary phase (slowly dividing) bacterial cultures. Given that bacteria reside in different metabolic states in infected tissues[21,22], PABA has the potential to detect slowly dividing or "dormant" bacteria *in vivo*. Together these qualities of specific uptake in diverse micro- organisms, clinical strains including MDROs and low tissue background, make ^{11}C-PABA an attractive candidate for infection imaging.

In this study, we developed a convenient radiosynthesis of α-[^{11}C]PABA (^{11}C-PABA) from a commercially available Grignard precursor. We then showed accumulation of ^{11}C-PABA into *E. coli* and *S. aureus* laboratory strains, and applied it to a simple model of murine infection.

Results and Discussion

Synthesis of [^{11}C]PABA has not previously been described, so we developed a novel synthetic method for production and purification of [^{11}C]PABA starting from a commercially available Grignard precursor (Figure 2). [^{11}C]PABA was isolated in 35% decay-corrected radiochemical yield (RCY) and >99% radiochemical purity (RCP) with a molar activity of 820 +/− 258 mCi/umol (n=4) at the end of synthesis. Product identity was confirmed via HPLC (Supp Fig 1–6), that included analysis using two stationary/mobile phase combinations.

To show that PABA was efficiently incorporated into both gram-negative and gram-positive bacteria we incubated cultures of *E. coli* and *S. aureus* with [^{11}C]PABA and measured its incorporation at time points of 20, 40 and 60 minutes. *In vitro* data were normalized to the number of colony-forming units via serial dilution and plating. Both live *E. coli* and *S. aureus* exhibited increased radiotracer uptake/accumulation as the incubation time increased (Figure 3). At 60 minutes incubation time, uptake of [^{11}C]PABA was significantly higher in both live *E. coli* (p<0.0001) and *S. aureus* (p<0.0001) when compared to heat-killed *E. coli* and *S. aureus*, respectively (> 10-fold difference at 60 minutes), suggesting that uptake is specific for live bacteria. Excess cold PABA in a much higher concentration (2 mM) blocked uptake of [^{11}C]PABA in both *E. coli* (p<0.0001) and *S. aureus* (p<0.0001) suggesting intracellular transport of PABA was specific and could be saturated.

We further investigated the accumulation of PABA-derived metabolites *in vitro* via ^{13}C and ^{1}H NMR, taking advantage of the high metabolite specificity of chemical shift. The experiment was designed carefully to match the media, organism (*E. coli* strain ATCC 25922), optical density (OD$_{600}$), and incubation time of the ^{11}C data. [α-^{13}C]PABA was synthesized using an analogous method to that used for [^{11}C]PABA at high yield (73%) and characterized via NMR and high-resolution mass spectrometry (HRMS) (Supp Fig 7). Following incubation in an exponential phase *E. coli* culture, the media concentration of [^{13}C]PABA was seen to decrease from an initial concentration of 5 mM to 1.7 mM in one hour, as determined using ^{1}H NMR in the presence of a tetramethylsilane (TMS) standard. *E. coli* extracts were subsequently analyzed via ^{13}C and ^{1}H NMR at 800 MHz alongside PABA and folate standards to determine the presence of enriched intracellular metabolites (Supp Fig 8,9). Interestingly, the dominant species seen was [^{13}C]PABA itself; in contrast no enriched folate products were seen. These data suggest that the accumulation of ^{11}C signal *in vivo*, studied subsequently, is also likely via intracellular retention of [^{11}C]PABA. An important caveat in interpreting these data is the significant difference in kinetic regimes for ^{11}C versus ^{13}C metabolites, with the ^{13}C PABA study representing a greater than 10^6-fold higher concentration.

To determine whether [^{11}C]PABA was a useful agent for differentiating living organisms from heat-killed bacteria *in vivo*, we employed a murine myositis model similar to one that has been previously reported[10,16]. This model is generated via simultaneous intramuscular inoculation of living versus heat-killed bacteria at different sites, to induce infection versus sterile inflammation. Confirmations of the validity of this model included both reproducing previously reported *in vivo* results using ^{18}F-FDS, and performing postmortem tissue homogenization and plating to confirm the presence of living bacteria. Immunocompetent mice were inoculated with live *E. coli* in the left deltoid muscle and a 10-fold higher concentration of heat-killed bacteria in the contralateral deltoid to incite sterile inflammation. After the infection was allowed to progress for 8 hours, mice were initially imaged by micro PET-CT using a dynamic acquisition (Supp Fig 10) to determine the optimum time point for static studies. Subsequent analysis was performed using a single time-point study similar to clinical protocols for [^{18}F]FDG. [^{11}C]PABA specifically accumulated in the infected left shoulder, while no detectable accumulation above background was observed in heat-killed inoculated right deltoid. A representative coronal image is shown in Figure 4A, with an axial image shown in Supp Fig 11. Spherical regions-

of-interest (ROIs) were drawn to quantify the accumulation of PABA in the infected deltoid, the contralateral heat-killed inoculation site, and normal muscle. ROI analysis showed [^{11}C]PABA produced 2.6-fold higher counts (N=4, p = 0.0286) in the shoulder inoculated with live *E. coli* as compared to heat-killed inoculation (Figure 4B). These findings were corroborated by biodistribution analysis using a gamma counter following euthanasia, which showed an significant (N=5, p = 0.0178) difference in [^{11}C]PABA accumulation in infected versus heat-killed sites, where tracer retention was similar to normal muscle (p > 0.9999). (Figure 4C). Postmortem tissue histology (hematoxylin and eosin, Gram-stain) was performed to verify presence of structurally intact bacteria in the infected deltoid, and inflammatory cells without bacteria in the contralateral uninfected deltoid. Representative data for *E. coli* inoculations (n=4 animals studied) are shown in Figure 4D. To further document the presence of inflammation at heat-killed sites, and show the potential advantages of [^{11}C]PABA, we studied a cohort of *E. coli*-infected animals using ^{18}F-FDG (Supp Fig 12–13). By both ROI and *ex vivo* analyses, live versus heat-killed inoculation sites showed no significant differences in tracer accumulation, but both showed increases with respect to background (normal muscle). These findings are highly consistent with previous reports using this model, that also found no statistically significant differences in ^{18}F-FDG accumulation between living versus heat-killed sites[10,16].

These findings suggest that [^{11}C]PABA is an attractive candidate for imaging living bacteria in humans. One major strength is the broad sensitivity of PABA for human pathogens. ^{3}H-PABA has shown incorporation into model pathogens representing several important bacterial classes: *S. aureus* (gram-positive), *E. coli* (gram-negative, Enterobacteriaceae), *Pseudomonas aeruginosa* (gram-negative, non-Enterobacteriaceae), and mycobacteria[20]. Another potential strength is the short half-life of [^{11}C]PABA (~20 minutes), which could allow repeat tracer doses (and imaging) over a short time interval. Thus [^{11}C]PABA might be administered twice with intervening antibiotics for rapid determination of treatment effect.

However, this short half-life would also limit the clinical application of [^{11}C]PABA to facilities with an on-site cyclotron. Therefore, discovery of ^{18}F-derived PABA radiotracers, that mimic the features of the endogenous substrate, would represent a key development. In addition, we only noted a modest signal-to-background ratio (~3 fold) in infected mouse tissues when compared to sites of heat-killed inoculaton. This is presumably due to the short biological half-life and thus exposure of [^{11}C]PABA to the infected sites in mice. Given more favorable pharmacokinetics of PABA in larger animals, including humans, we anticipate much better signal-to-noise in clinical settings[23].

Finally, [^{11}C]PABA-PET images would need to be interpreted in the context of the normal human microbiome[24]. The commensal bacteria present in human skin and aerodigestive tract (lungs, bowel, etc.) would likely also accumulate [^{11}C]PABA or related tracers. Fortunately, the spatial information provided by PET (and other tomographic imaging modalities) can usually distinguish between potential sites of infection and uptake that is likely due to normal flora. Bacteria-specific radiotracers might be applied most effectively to infections of normally sterile spaces, which can be very difficult to sample, diagnose and treat. These include important musculoskeletal infections (vertebral discitis-osteomyelitis, large joint

septic arthritis, diabetic foot) and hepatobiliary infections (cholangitis, infected pancreatic pseudocysts)[25–28]. Several of these locations are also difficult to sample both in terms of risks and often expensive surgical biopsies, highlighting the value of improved diagnostic methods. In the future, we hope to leverage [^{11}C]PABA and other metabolic tools to better diagnose the presence, location, type, and antimicrobial susceptibility of pathogenic microorganisms.

Materials and Methods

Radiochemical synthesis of [^{11}C]PABA

Cyclotron-generated [^{11}C]CO_2 was delivered into a 300 μL solution of 4-[Bis(trimethylsilyl)amino] phenylmagnesium bromide (0.5 M in THF, Sigma Aldrich) at a rate of 50 mL/min using argon carrier gas and allowed to react for 2 minutes at room temperature. The THF/Grignard solution was subsequently quenched with hydrochloric acid (150 μL of 1 M HCl diluted with 3 mL of 15 mM phosphate buffer) and loaded onto a Synergi Hydro-RP semi-preparative High-Performance Liquid Chromatography (HPLC) system. The desired product was eluted using a 95% phosphate buffer (20 mM, pH = 8.0), 5% ethanol mobile phase and analyzed via a Synergi Hydro-RP analytic column under identical conditions. For a complete description of the procedure and additional chromatograms, please refer to the Supplementary Information.

[^{11}C]PABA uptake studies

E. coli (strain ATCC 25922, VWR) and *S. aureus* (strain ATCC 12600, VWR) were cultured in LB Broth to an optical density at 600 nm (OD_{600}) of 1.0. Heat-killed samples were prepared by incubating 1 mL aliquots of bacterial culture for 30 minutes at 90 °C. Samples from both live and heat-killed bacteria were serially diluted and plated on LB agar plates to determine the concentration of colony forming units (CFU) for each condition. 1 mL aliquots of live or heat-killed bacterial cultures were incubated with 1 μCi of [^{11}C]PABA (3 replicates for each condition). For blocking experiments, cold (nonradioactive) PABA was also added to the culture to a final concentration of 2 mM. The culture tubes were incubated at 37°C until the desired time point. Bacteria were then pelleted and supernatant was aspirated. Bacteria were resuspended in 1 mL of ice-cold Phosphate-Buffered Saline (PBS) and re-pelleted 3 times each to thoroughly wash the samples. Retained radiotracer within the samples was then counted on an Automated Gamma Counter (Hidex, Turku, Finland.)

Animals and experimental design

The Institutional Animal Care and Use Committee at UCSF approved all procedures. The UCSF Laboratory Animal Resource Center (LARC) provided veterinary services for the study and all studies were performed in accordance with UCSF guidelines regarding animal housing, pain management, and euthanasia. All mice used were CBA/J females (Jackson Laboratory) aged between 8–10 weeks. LB cultures were inoculated with single colonies of *E. coli* and were placed in an oscillating incubator (~120 rpm) at 37 °C until they reached OD_{600} of 1.0 (approximately 12–14h). For heat-killed samples, 1 mL aliquots of the culture were incubated at 90 °C for 30 minutes and then pelleted by centrifugation and resuspended in 100 μL of LB broth. Mice were placed under isoflurane anesthesia on a warming pad and

100 μL of live bacterial culture and 100 μL of 10X concentrated heat-killed bacteria were injected with tuberculin syringes into the right and left shoulder musculature, respectively. Mice were then removed from anesthesia, allowed to recover, and intermittently monitored prior to imaging. Imaging of *E. coli*-infected mice was initiated at approximately 8 hours following inoculation for [^{11}C]PABA studies.

PET imaging

Under isoflurane anesthesia, a tail vein catheter was placed. Approximately 1 mCi of [^{11}C]PABA was injected via the tail vein catheter. The animals were placed on a heating pad to minimize shivering. Mice were allowed to recover, micturate, and at 45 minutes post-injection, placed back under isoflurane anesthesia and the animals were transferred to a Siemens Inveon micro PET-CT system (Siemens, Erlangen, Germany). PET images were obtained using a single static 15 min acquisition followed by micro-CT scan for attenuation correction and anatomical co-registration. No adverse events were observed during or after injection of any compound. Anesthesia was maintained during imaging using isoflurane.

Biodistribution assays

Upon completion of imaging, mice were sacrificed and biodistribution analysis performed using harvested deltoid muscle. Non-inoculated normal thigh muscle was also harvested as a control. Gamma counting of harvested tissues (n=4) was performed using a Hidex Automatic Gamma Counter (Turku, Finland).

Data analysis and statistical considerations

All PET data were viewed using open source Amide software (amide.sourceforge.net)[29]. Quantification of uptake was performed by drawing regions of interest over indicated organs on the CT images, and expressed as percent injected dose per cubic centimeter (cc). All statistical analysis was performed using Graphpad Prism 7d (La Jolla, CA). *In vitro* [^{11}C]PAPA uptake data were analyzed using two-way analysis of variance (ANOVA) with Tukey's multiple comparison test. *Ex vivo* biodistribution data were analyzed using the Kruskal-Wallis test followed by Dunn's multiple comparison test. ROI analysis data were analyzed using the Mann-Whitney test. For all statistical tests, p value were adjusted for multiple comparisons, and less than 0.05 was considered statistically significant. All graphs are depicted with error bars corresponding to standard deviation.

Histopathology

Muscle tissues inoculated with heat-killed or live bacteria were fixed overnight in 4% paraformaldehyde before being sequentially dehydrated and embedded in paraffin. Paraffin embedded tissues were sectioned on a microtome at 4μm and stained with hematoxylin and eosin (H&E) or Gram-stain.

Supplementary Material

Refer to Web version on PubMed Central for supplementary material.

Acknowledgments

References

1. Palestro CJ. Radionuclide imaging of osteomyelitis. Semin Nucl Med. 2015; 45:32–46. DOI: 10.1053/j.semnuclmed.2014.07.005 [PubMed: 25475377]

2. Gafter-Gvili A, Raibman S, Grossman A, Avni T, Paul M, Leibovici L, Tadmor B, Groshar D, Bernstine H. [18F]FDG-PET/CT for the diagnosis of patients with fever of unknown origin. QJM. 2015; 108:289–298. DOI: 10.1093/qjmed/hcu193 [PubMed: 25208896]

3. Bleeker-Rovers CP, Vos FJ, van der Graaf WTA, Oyen WJG. Nuclear medicine imaging of infection in cancer patients (with emphasis on FDG-PET). Oncologist. 2011; 16:980–991. DOI: 10.1634/theoncologist.2010-0421 [PubMed: 21680576]

4. Carr C, Diehn F, Kaufmann T. Nonenhancing epidural abscess and discitis in an immunocompromised patient: a case report. Clin Neurol Neurosurg. 2013; 115:2274–2276. DOI: 10.1016/j.clineuro.2013.07.018 [PubMed: 23937866]

5. Vos FJ, Donnelly JP, Oyen WJG, Kullberg BJ, Bleeker-Rovers CP, Blijlevens NMA. 18F-FDG PET/CT for diagnosing infectious complications in patients with severe neutropenia after intensive chemotherapy for haematological malignancy or stem cell transplantation. Eur J Nucl Med Mol Imaging. 2012; 39:120–128. DOI: 10.1007/s00259-011-1939-1 [PubMed: 21947022]

6. Blaser M. Antibiotic overuse: Stop the killing of beneficial bacteria. Nature. 2011; 476:393–394. DOI: 10.1038/476393a [PubMed: 21866137]

7. Khabbaz RF, Moseley RR, Steiner RJ, Levitt AM, Bell BP. Challenges of infectious diseases in the USA. The Lancet. 2014; 384:53–63. DOI: 10.1016/S0140-6736(14)60890-4

8. Lawal I, Zeevaart J, Ebenhan T, Ankrah A, Vorster M, Kruger HG, Govender T, Sathekge M. Metabolic imaging of infection. J Nucl Med. 2017; 58:1727–1732. DOI: 10.2967/jnumed.117.191635 [PubMed: 28818989]

9. Sriram R, Sun J, Villanueva-Meyer J, Mutch C, De Los Santos J, Peters J, Korenchan DE, Neumann K, Van Criekinge M, Kurhanewicz J, et al. Detection of Bacteria-Specific Metabolism Using Hyperpolarized [2-13C]Pyruvate. ACS Infect Dis. 2018; doi: 10.1021/acsinfecdis.7b00234

10. Weinstein EA, Ordonez AA, DeMarco VP, Murawski AM, Pokkali S, MacDonald EM, Klunk M, Mease RC, Pomper MG, Jain SK. Imaging Enterobacteriaceae infection in vivo with 18F-fluorodeoxysorbitol positron emission tomography. Sci Transl Med. 2014; 6:259ra146.doi: 10.1126/scitranslmed.3009815

11. Namavari M, Gowrishankar G, Hoehne A, Jouannot E, Gambhir SS. Synthesis of [^{18}F]-labelled maltose derivatives as PET tracers for imaging bacterial infection. Mol Imaging Biol. 2015; 17:168–176. DOI: 10.1007/s11307-014-0793-5 [PubMed: 25277604]

12. Gowrishankar G, Hardy J, Wardak M, Namavari M, Reeves RE, Neofytou E, Srinivasan A, Wu JC, Contag CH, Gambhir SS. Specific Imaging of Bacterial Infection Using 6 -18F-Fluoromaltotriose: A Second-Generation PET Tracer Targeting the Maltodextrin Transporter in Bacteria. J Nucl Med. 2017; 58:1679–1684. DOI: 10.2967/jnumed.117.191452 [PubMed: 28490473]

13. Petrik M, Zhai C, Haas H, Decristoforo C. Siderophores for molecular imaging applications. Clin Transl Imaging. 2017; 5:15–27. DOI: 10.1007/s40336-016-0211-x [PubMed: 28138436]

14. Vorster M, Maes A, Wiele C, van de Sathekge M. Gallium-68 PET: A Powerful Generator-based Alternative to Infection and Inflammation Imaging. Semin Nucl Med. 2016; 46:436–447. DOI: 10.1053/j.semnuclmed.2016.04.005 [PubMed: 27553469]

15. Ioppolo JA, Caldwell D, Beiraghi O, Llano L, Blacker M, Valliant JF, Berti PJ. 67Ga-labeled deferoxamine derivatives for imaging bacterial infection: Preparation and screening of functionalized siderophore complexes. Nucl Med Biol. 2017; 52:32–41. DOI: 10.1016/j.nucmedbio.2017.05.010 [PubMed: 28602965]

16. Neumann KD, Villanueva-Meyer JE, Mutch CA, Flavell RR, Blecha JE, Kwak T, Sriram R, VanBrocklin HF, Rosenberg OS, Ohliger MA, et al. Imaging Active Infection in vivo Using D-

Amino Acid Derived PET Radiotracers. Sci Rep. 2017; 7:7903.doi: 10.1038/s41598-017-08415-x [PubMed: 28801560]

17. Brown GM. The biosynthesis of folic acid. II. Inhibition by sulfonamides. J Biol Chem. 1962; 237:536–540. [PubMed: 13873645]

18. Sellmyer MA, Lee I, Hou C, Weng CC, Li S, Lieberman BP, Zeng C, Mankoff DA, Mach RH. Bacterial infection imaging with [18F]fluoropropyl-trimethoprim. Proc Natl Acad Sci USA. 2017; 114:8372–8377. DOI: 10.1073/pnas.1703109114 [PubMed: 28716936]

19. Johansson G, Bingham S, Vahter M. A method to compensate for incomplete 24-hour urine collections in nutritional epidemiology studies. Public Health Nutr. 1999; 2:587–591. [PubMed: 10656479]

20. Ordonez AA, Weinstein EA, Bambarger LE, Saini V, Chang YS, DeMarco VP, Klunk MH, Urbanowski ME, Moulton KL, Murawski AM, et al. A Systematic Approach for Developing Bacteria-Specific Imaging Tracers. J Nucl Med. 2017; 58:144–150. DOI: 10.2967/jnumed.116.181792 [PubMed: 27635025]

21. Ordonez AA, Tasneen R, Pokkali S, Xu Z, Converse PJ, Klunk MH, Mollura DJ, Nuermberger EL, Jain SK. Mouse model of pulmonary cavitary tuberculosis and expression of matrix metalloproteinase-9. Dis Model Mech. 2016; 9:779–788. DOI: 10.1242/dmm.025643 [PubMed: 27482816]

22. Murawski AM, Gurbani S, Harper JS, Klunk M, Younes L, Jain SK, Jedynak BM. Imaging the evolution of reactivation pulmonary tuberculosis in mice using 18F-FDG PET. J Nucl Med. 2014; 55:1726–1729. DOI: 10.2967/jnumed.114.144634 [PubMed: 25082854]

23. Mordenti J. Man versus beast: pharmacokinetic scaling in mammals. J Pharm Sci. 1986; 75:1028–1040. [PubMed: 3820096]

24. Young VB. The role of the microbiome in human health and disease: an introduction for clinicians. BMJ. 2017; 356:j831.doi: 10.1136/bmj.j831 [PubMed: 28298355]

25. Duarte RM, Vaccaro AR. Spinal infection: state of the art and management algorithm. Eur Spine J. 2013; 22:2787–2799. DOI: 10.1007/s00586-013-2850-1 [PubMed: 23756630]

26. Mathews CJ, Weston VC, Jones A, Field M, Coakley G. Bacterial septic arthritis in adults. The Lancet. 2010; 375:846–855. DOI: 10.1016/S0140-6736(09)61595-6

27. Lee JG. Diagnosis and management of acute cholangitis. Nat Rev Gastroenterol Hepatol. 2009; 6:533–541. DOI: 10.1038/nrgastro.2009.126 [PubMed: 19652653]

28. Forsmark CE, Vege SS, Wilcox CM. Acute Pancreatitis. N Engl J Med. 2016; 375:1972–1981. DOI: 10.1056/NEJMra1505202 [PubMed: 27959604]

29. Loening AM, Gambhir SS. AMIDE: a free software tool for multimodality medical image analysis. Mol Imaging. 2003; 2:131–137. [PubMed: 14649056]
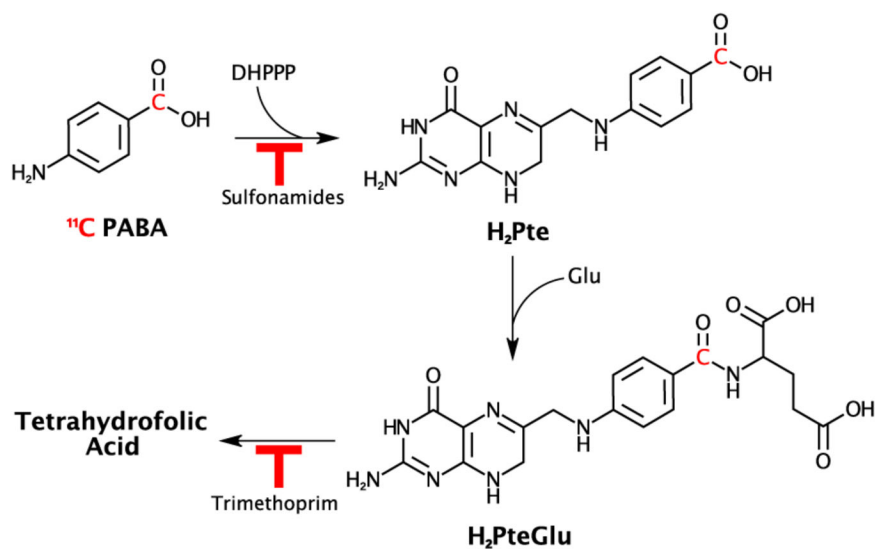
Figure 1. Folate biosynthesis pathway and possible incorporation sites of [^{11}C]PABA
The chemical structure of [^{11}C]PABA is shown with the ^{11}C radionucleus highlighted in red. Pathways inhibited by common sulfonamide antibiotics and trimethoprim are also shown. The first step, incorporation of PABA into dihydropteroate via dihydropteroate synthase (EC 2.5.1.15) via condensation with 2-amino-4-hydroxy-7,8-dihydropterin-6-yl)methyl diphosphate is the site of action of sulfonamide antibiotics. Following incorporation of glutamate to form dihydrofolate, trimethoprim inhibits reduction to tethrahydrofolate. DHPPP = 2-amino-4-hydroxy-7,8-dihydropterin-6-yl)methyl diphosphate, H_2Pte = dihydropteroate, Glu = glutamate, H_2PteGlu = dihydrofolate.
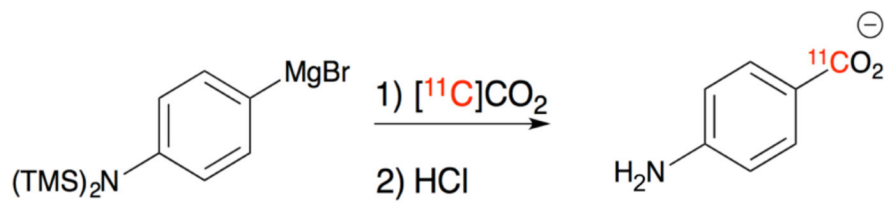
Figure 2. Radiosynthesis of [^{11}C]PABA
(a) Radiosynthesis of [^{11}C]PABA via [^{11}C]CO$_2$ and a commercially available Grignard precursor followed by quenching in aqueous HCl.
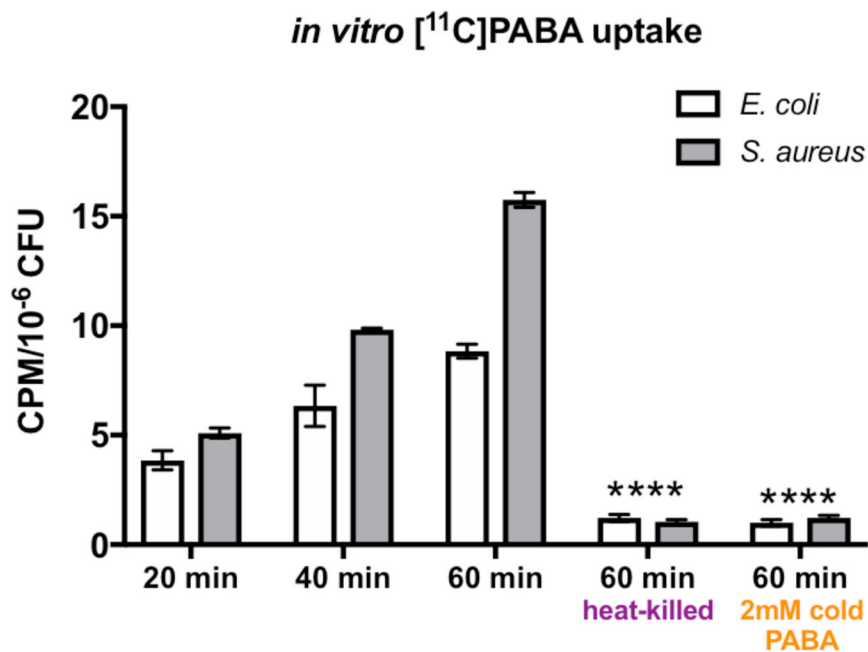
Figure 3. In vitro uptake of [11C]PABA

1 μCi of [11C]PABA was incubated in 1 mL culture of *E. coli* (white bars) or *S. aureus* (gray bars) for 20, 40 or 60 minutes. Accumulation of the tracer relative to colony-forming units (CFUs) was determined by serial dilution and plating. As the incubation time increases, both live E. coli and S. aureus exhibited increased radiotracer uptake. At 60 minutes, there was significantly higher uptake in live *E. coli* and *S. aureus* than heat-killed *E. coli* and *S. aureus*, respectively(****$p < 0.0001$ for both bacteria). Uptake of [11C]PABA was effectively blocked in both live *E. coli* and *S. aureus* by an excess of 2mM cold PABA, shown by significantly lower radiotracer signal at 60 minutes than regular incubation (****$p < 0.0001$ for both bacteria).
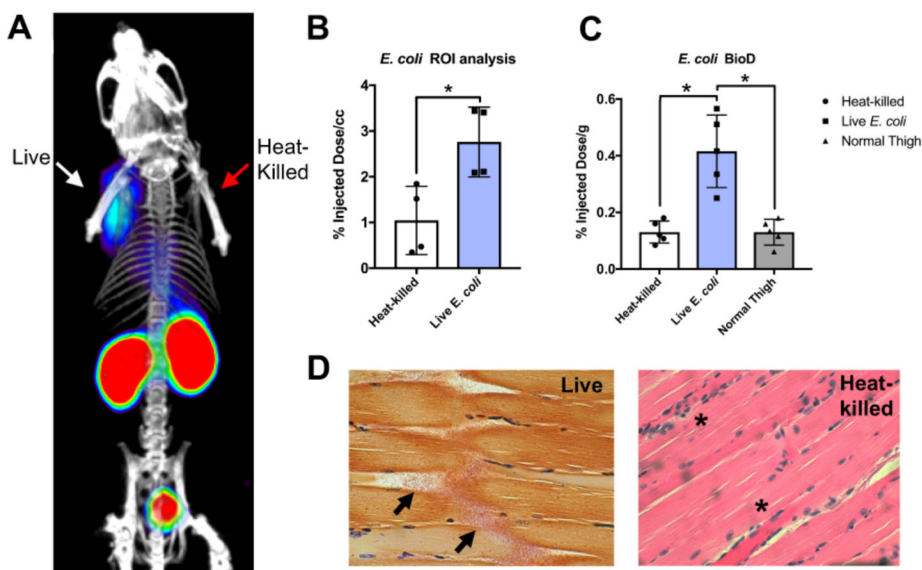
Figure 4. [^{11}C]PABA PET can differentiate active bacterial infection from sterile inflammation *in vivo*

(a) Representative microPET/CT image acquired in a murine myositis model using [^{11}C]PABA (n=4 animals described in this study). The left side of the image corresponds to deltoid muscle inoculated with live *E. coli*, while the right side corresponds to inoculation with 10-fold greater (10X) heat-killed bacteria. This image highlights the specificity of [^{11}C]PABA for living bacteria, its primary renal excretion, and the low background in most tissues. (b) ROI analysis of PET images showed a significantly (*p = 0.0286) higher radiotracer uptake (expressed in percent injected dose per cubic centimeter (%ID/cc) in infection sites induced by live *E. coli* than sterile inflammation sites induced by heat-killed *E. coli*. (c) Biodistribution analysis using a gamma counter was performed on harvested tissues to corroborate ROI findings. This study showed a significant (*p = 0.0178) difference in [^{11}C]PABA retention in live versus heat-killed inoculation sites, which showed tracer retention similar to normal muscle (p > 0.9999). (d) Histologic analysis of harvested deltoid muscles. The left panel corresponds to a Gram-stain of muscle infected with living *E. coli*, with arrows highlighting morphologically intact bacteria infiltrating muscle fibers. The right panel shows deltoid muscle stained with hematoxylin and eosin (H&E) corresponding to inoculation with heat-killed bacteria. Intact bacteria are not seen, but numerous inflammatory cells are present (highlighted by *).